Int. J. Multiphase Flow Vol. 16, No. 2, pp. 295–304, 1990
Printed in Great Britain.

0301-9322/90 $3.00 + 0.00

APPROXIMATE ANALYSIS OF INTERACTING VAPORIZING FUEL DROPLETS

C. KLEINSTREUER† and T.-Y. WANG
Department of Mechanical and Aerospace Engineering, North Carolina State University, Raleigh, NC 27695-7910, U.S.A.

(*Received* 12 *January* 1989; *in revised form* 25 *September* 1989)

Abstract—An accurate analysis and effective computer simulation of evaporating droplets moving through a stagnant hot gas are important for the understanding of the basic process dynamics, as well as for improvement of global spray models and specific spray models and specific dispersed-flow-system designs. Using input data for the gasification of three *n*-decane fuel droplets, the transient interaction effects on the individual droplet Reynolds numbers, vaporization rates, droplet distances and average Nusselt numbers have been analyzed for different initial conditions. The present work is an extension of our experimentally verified boundary-layer analysis of a single vaporizing droplet, assuming laminar axisymmetric flow and spherically shrinking droplets. The computer simulation model can be used to find optimal operational conditions to achieve rapid gasification without droplet collisions.

Key Words: two-phase flow, multiple vaporizing fuel droplets, interaction effects, boundary-layer analysis

1. INTRODUCTION

A detailed and accurate approximate analysis of the dynamics and transport mechanisms of multiple, interacting vaporizing droplets in a hot gas stream is important for the basic understanding and improvement of a variety of two-phase flow systems. Applications include spray processes, such as fuel droplet combustion or spray cooling, and discrete particle/fluid flow interactions such as particle-laden jets or particle suspension flows.

The problem of thermal convection past a spherical particle has attracted numerous investigators (cf. Kuo 1986; Clift *et al.* 1978 etc.). For example, Finlayson & Olson (1987) developed accurate Nusselt number correlations for single spheres. Kleinstreuer & Wang (1988) analyzed the heat transfer mechanisms between rotating porous spheres and flowing power-law fluids. The problem of single-droplet vaporization in a convective gas stream has been addressed by Prakash & Sirignano (1980), Prakash & Krishan (1984), Abramson & Sirignano (1988) and Renksizbulut & Haywood (1988), among others. Thermal convection studies of multiple interacting particles are restricted to two-sphere/droplet systems with the exception of the fluid mechanics and heat transfer simulations of three closely-spaced spheres by Ramachandran *et al.* (1980a, b). For example, Raju & Sirignano (1987) combined the finite difference code developed by Dwyer & Sanders (1984) with the grid transformation scheme published by Thomson *et al.* (1977), to solve the unsteady Navier–Stokes equations ($Re_d \leqslant 100$) for two vaporizing droplets in tandem. Relevant experimental work is confined to flow visualization and measurements of the individual drag coefficients and flow separation angles of two-sphere systems (e.g. Rowe & Henwood 1961; Tsuji *et al.* 1982).

In order to contribute to a more realistic simulation of dense–dispersed flow, at least three to five dynamically interacting droplets with phase change in the moderate-to-high Reynolds number regime have to be considered (cf. Ramachandran & Kleinstreuer 1986). In this paper, the approximate analysis by Wang & Kleinstreuer (1989) is extended to multiple dynamically interacting vaporizing droplets at $Re_{d0} \geqslant 100$. Results are shown for three droplets, employing a modified form of the correlations for the drag/interaction coefficients of three closely-spaced spheres/droplets developed by Ramachandran *et al.* (1989a), and a thermal near-wake model deduced from the work by Ramachandran *et al.* (1989b) The assumptions of laminar axisymmetric boundary-layer flow for $Re_{d0} \geqslant 100$, quasi-steady-state gas-phase dynamics, negligible internal droplet circulation and droplet sphericity are discussed in Wang & Kleinstreuer (1989).

†To whom all correspondence should be addressed.

2. ANALYSIS

Considering three spherical droplets on a one-dimensional trajectory, the dynamics of the jth droplet is described by Newton's second law of motion (figure 1):

$$\frac{dw_j}{dt} = -\frac{3}{4}\frac{C_{D,j}}{d_j}\frac{\rho_a}{\rho_p}|w_j|w_j, \qquad j = 1, 2, 3, \tag{1a}$$

subject to

$$z_j = z_{j,0} \quad \text{and} \quad w_j = w_{j,0} \qquad \text{at } t = 0. \tag{1b}$$

Here, w_j is the velocity of droplet j, t is the time, d is the droplet diameter, C_D is the effective drag coefficient, ρ is the density for the gas mixture (ρ_a) or the droplet (ρ_p) and z is the axial coordinate.

At any time step, the dimensionless droplet distance is

$$d_{j,j+1} = \frac{z_j - z_{j+1}}{d_0}, \qquad j = 1, 2, \tag{2}$$

where the velocity of the jth droplet is

$$w_j = \frac{dz_j}{dt}. \tag{3}$$

The $C_{D,j}$s represent the effective drag force on the jth particle due to its motion and the presence of the other (two) particles (Ramachandran *et al.* 1989a). Presently, the effect of droplet vaporization (i.e. surface blowing) on $C_{D,j}$ is not yet incorporated. Hence, only the initial dimensionless time period, $\tau_G \leqslant 10$, of the droplet dynamics is shown. The correlations are with $Re_d = wd/\nu_\infty$:

$$\frac{C_{D,1}}{(C_{Ds})_1} = -1 - 0.096(Re_d)_1^{0.2475} d_{12}^{-0.965} \exp\left(\frac{0.4764}{d_{23}}\right), \tag{4}$$

$$\frac{C_{D,2}}{(C_{Ds})_2} = 1 - (Re_d)_2^{0.1593}\,(0.2932 d_{12}^{-0.4876} + 0.1341 d_{23}^{-0.4242}) \tag{5}$$

and

$$\frac{C_{D,3}}{(C_{Ds})_3} = 1 - 0.325[\ln(Re_d)_3 + 1]^{0.603} d_{23}^{-0.385} \exp\left(\frac{-0.282}{d_{12}}\right), \tag{6}$$

where the standard drag correlation for the solitary droplet is (White 1974):

$$(C_{Ds})_j = \frac{24}{(Re_d)_j} + \frac{6}{1 + \sqrt{(Re_d)_j}} + 0.4. \tag{7}$$

An inertial coordinate frame is employed, where at each time level the orthogonal x–y coordinate system is fixed to the individual droplets (cf. figure 1). The streamwise coordinate x is measured along the surface from the forward stagnation point and y is the coordinate normal to the surface; r is the distance from the axis of symmetry to the drop surface; u and v are the gas-phase velocity

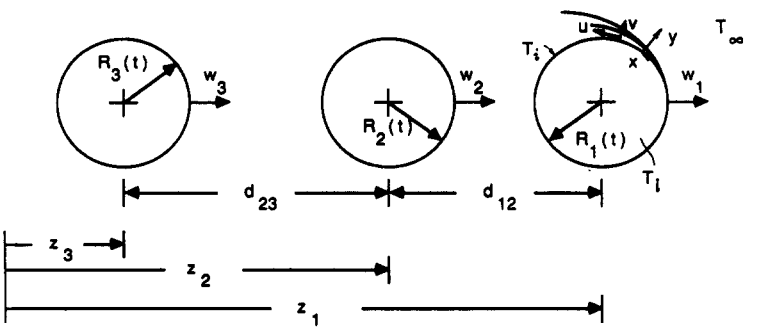

Figure 1. System schematics and coordinates.

components; h is the enthalpy of the gaseous mixture; T is the temperature; Y is the vapor mass fraction; A is the droplet area, λ is the gas constant and L is the latent heat; k, $\mathscr{D}$ and α are the conductivity, the mass diffusion coefficient and the thermal diffusivity, respectively; subscripts b, e, G, i, L and 0 indicate boiling, boundary-layer edge, gas phase, interface, liquid-phase and initial conditions, respectively. Hence, the gas-phase fluid mechanics, liquid-phase heating and droplet vaporization can be described by (Wang & Kleinstreuer 1989):

(continuity)
$$\frac{\partial(r\rho u)}{\partial x}+\frac{\partial(r\rho v)}{\partial y}=0, \qquad [8]$$

(momentum)
$$\rho\left(u\frac{\partial u}{\partial x}+v\frac{\partial u}{\partial y}\right)=\rho_e u_e\frac{\mathrm{d}u_e}{\mathrm{d}x}+\frac{\partial}{\partial y}\left(\mu\frac{\partial u}{\partial y}\right), \qquad [9]$$

(energy)
$$\rho\left(u\frac{\partial h}{\partial x}+v\frac{\partial h}{\partial y}\right)=\frac{\partial}{\partial y}\left(k\frac{\partial T}{\partial y}\right), \qquad [10]$$

(species)
$$\rho\left(u\frac{\partial Y}{\partial x}+v\frac{\partial Y}{\partial y}\right)=\frac{\partial}{\partial y}\left(\rho\mathscr{D}\frac{\partial Y}{\partial y}\right), \qquad [11]$$

(conduction)
$$\frac{\partial T_L}{\partial t}=\frac{\alpha_L}{r^2}\frac{\partial}{\partial r}\left(r^2\frac{\partial T_L}{\partial r}\right), \qquad [12]$$

(mass flux)
$$(\rho v)_i(Y_i-1)=\left(\rho\mathscr{D}\frac{\partial Y}{\partial y}\right)_i \qquad [13]$$

and

(heat flow)
$$(\rho v)_i AL+\left(k_L A\frac{\partial T_L}{\partial r}\right)_i=\left(k_G A\frac{\partial T}{\partial y}\right)_i. \qquad [14]$$

The associated gas-phase boundary conditions are:

at $y=0$,
$$u=0,\quad v=v_i,\quad T=T_i,\quad Y=Y_i; \qquad [15a]$$

and

at $y\to\infty$,
$$u=u_e(x),\quad T=T_\infty,\quad Y=Y_\infty=0. \qquad [15b]$$

The liquid-phase conditions are:

$$T_L(t=0)=T_0 \qquad \forall r; \qquad [15c]$$

and

$$\left.\frac{\partial T_L}{\partial r}\right|_{r=0}=0,\quad \left.\frac{\partial T_L}{\partial r}\right|_{r=R(t)}\sim q_i. \qquad [15d]$$

The mass fraction at the interface is a function of the droplet surface temperature,

$$Y_i=\exp\left[\frac{L}{\lambda}\left(\frac{1}{T_b}-\frac{1}{T_i}\right)\right], \qquad [16]$$

and the time rate of change of the droplet radius can be expressed as

$$\frac{\mathrm{d}}{\mathrm{d}t}R(t)=\frac{1}{2\rho_L}\int_0^{\theta_s}(\rho v)_i\sin\theta\,\mathrm{d}\theta. \qquad [17]$$

The transformation and solution of [8]–[17] are given in Wang & Kleinstreuer (1989). Their experimentally verified computer code appears as a subroutine in the present model for the calculation of the interfacial conditions, and hence the droplet size at each time level (cf. figure 2). The dimensionless time is defined as $\tau_G=4tv_G/d^2$. In summary, a patched boundary-layer approximation is being employed to solve for (the) transfer processes of the droplets at each time step, i.e. the droplets are kept stationary and treated individually during each Δt.

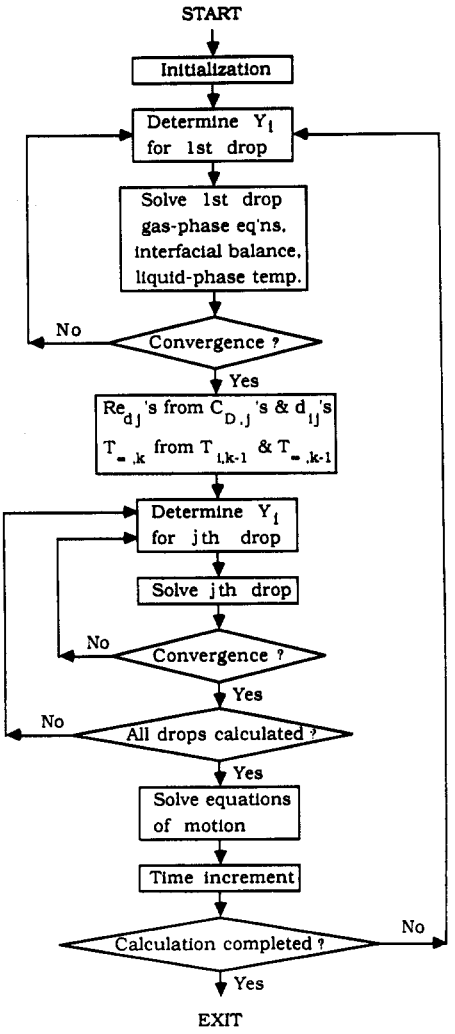

Figure 2. Computational flow chart.

3. NUMERICAL SOLUTION

Keller's box method has been extended to solve the system of gas-phase boundary-layer equations for momentum, heat and mass transfer simultaneously (cf. Wang & Kleinstreuer 1989). A different implicit finite difference scheme has been used to solve the liquid-phase transient conduction equation. After initialization of the program with an educated guess for the droplet surface temperature, the preliminary interfacial mass fraction can be obtained from [16] and the transformed versions of [8]–[11], subject to conditions [15a, b], are solved at each time step. Now the interfacial conditions [13] and [14] have to be fulfilled which yields a boundary condition, i.e. [15d], for the solution of [12]. Then the new droplet surface temperature is used in the solution of the gas-phase equations until, iteratively, convergance has been achieved, i.e. $\left|(T_i^{new} - T_i^{old})/T_i^{new}\right| \leqslant 10^{-4}$. The new droplet radius is obtained from [17]. Thus, the gas-side equations are solved for quasi-steady-state conditions, although the individual droplet radius changes with time, i.e. $R_j = R_j(t)$, $j = 1, 2, 3$.

Simultaneously, at any given time level, [1]–[3] are solved where the $C_{D,j}$ expressions [4]–[7] yield the effective approach stream Re_d for each droplet. The effective approach stream temperature is taken to be

$$T_{\infty,k+1} = 0.2T_{i,k} + 0.8T_{\infty,k}, \qquad k = 1, 2, \qquad [18]$$

based on the work by Ramachandran *et al.* (1989b). The computational flow chart for a multiple-droplet iterative procedure at each time step is given in figure 2.

Table 1. Comparison of the drag coefficient ratio ($C_{D,j}/C_{Ds}$) for flow past two tandem spheres; $Re_d = 40$

	$d_{12} = 1.5$			$d_{12} = 2$		$d_{12} = 4$	
	Tal *et al.* (1984)	Rowe & Henwood (1961)	Present method	Zapryanov & Toshev (1986)	Present method	Zapryanov & Toshev (1986)	Present method
First sphere	0.88	0.80	0.840	0.88	0.877	0.92	0.937
Second sphere	0.53	0.54	0.567	0.62	0.624	0.74	0.732

The accuracy of the computer simulation model is checked in two ways: (a) comparison of the predictive results with published experimental and theoretical data sets for specific case studies; and (b) testing of the mesh-independence of the results (cf. Wang & Kleinstreuer 1989).

4. RESULTS AND DISCUSSION

4.1. Model verification

The predictive capabilities of the core of the present computer simulation model have been successfully verified in the past with special case studies of mixed convectoin heat transfer of a sphere with blowing (cf. Kleinstreuer & Wang 1988) and single-droplet vaporization in a convective gas stream (Wang & Kleinstreuer 1989). Because of the lack of experimental or analytical results for three interacting particles, comparisons are made for two spheres/drops in tandem. Thus, correlations [4]–[6] are reduced for a two-sphere system by eliminating the effect of d_{23}, so that

$$\frac{C_{D,1}}{(C_{Ds})_1} = 1 - 0.096(Re_d)_1^{0.2475}\, d_{12}^{-0.965} \qquad [19]$$

and

$$\frac{C_{D,2}}{(C_{Ds})_2} = 1 - 0.2932(Re_d)_2^{0.1593}\, d_{12}^{-0.4876} \qquad [20]$$

A comparison of the computer predictions with both experimetnal data (Rowe & Henwood 1961) and numerical results (Zapryanov & Toshev 1986) is shown for different particle spacings in table 1. While table 1 summarizes individual drag coefficient ratios for closely-spaced spheres, figures 3 and 4 show for two interacting vaporizing droplets a comparison of the present results with the finite difference solution by Raju & Sirignano (1987). The input data used are listed in table 2. During the initial stage ($\tau_G \leqslant 10$), the amount of fuel evaporating is low and hence the droplet size reduction, as indicated with the temporal ratio of radii, is minor (figure 3a). However, Re_d decreases rapidly due to drag/interaction effects (figure 3b). The second droplet approaches the first one very quickly, as shown in figure 4. As indicated in table 1, the effective drag force is much lower for

Table 2. Input data sets for figures 3–10

	Raju & Sirignano (1987), figures 3a, 3b and 4	Present method (*n*-decane)
Operational data		
d_0 (μm)	50	50
$w_{j,0}$ (m/s)	25	25
T_∞ (K)	1000	1000
T_0 (K)	350	300
p (atm)	10	10
Fuel properties		
T_b (K)	573	565
ρ (kg/m^3)	NR	730
α (m^2/s)	NR	7.2×10^{-8}
$\mathscr{D}$ (m^2/s)	NR	1.155×10^{-8}
c_p (cal/g mol K)	NR	66
MW (g/g mol)	192	142.3
k (cal/s K)	NR	2.84×10^{-6}

NR ≅ not reported.

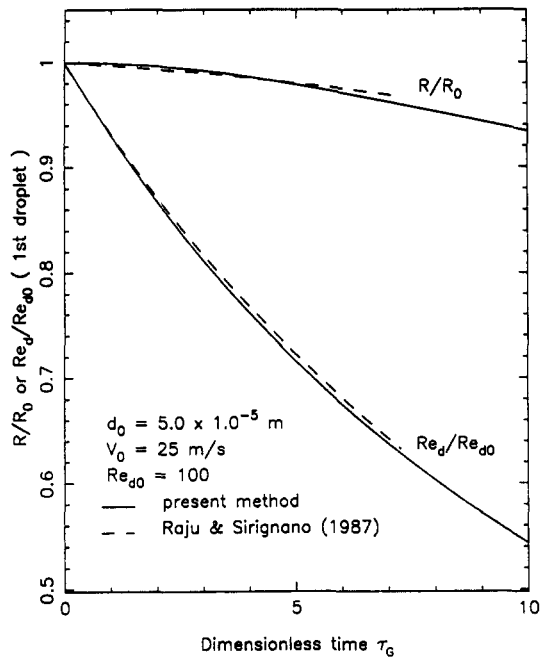

Figure 3a. Comparison of transient droplet radius and Reynolds number for the first droplet.

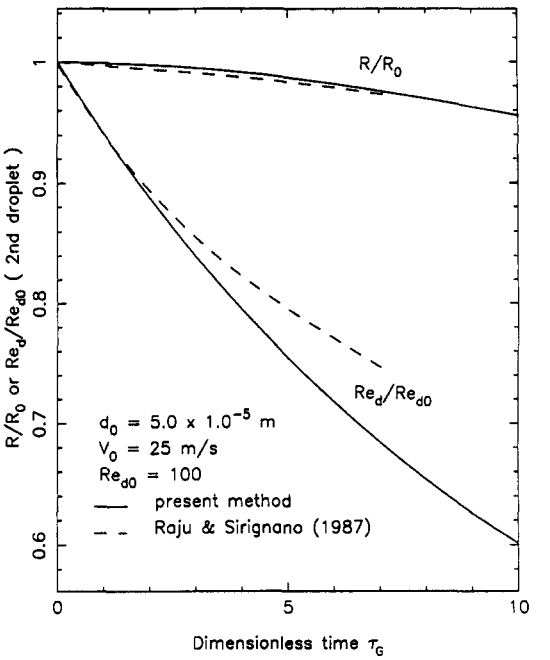

Figure 3b. Comparison of transient droplet radius and Reynolds number for the second droplet.

the second particle being in the wake of the leading particle and hence the faster moving second droplet catches up with the first droplet. The comparison of different system characteristics with the numerical results by Raju & Sirignano (1987) is very good for the two shrinking droplets (cf. figures 3a and 3b) and for the Re_d/Re_{d0} of the leading droplet (cf. figure 3a). However, Re_d for the second droplet and hence the droplet spacing differ (cf. figure 4). Since experimentally and theoretically verified drag/interaction coefficients have been employed in the present analysis, the discrepancies may be due to blowing effects, near-wake effects, and/or the use of different property values, not fully reported by Raju & Sirignano (1987) (cf. table 2).

4.2. Three-droplet dynamics

The transient changes in droplet radius, mass and Re_d for three dynamically interacting droplets are depicted in figures 5a–5c. While the transient characteristics of droplets 2 and 3 stay very similar, the first droplet shrinks faster and decelerates more rapidly. As a result, the second and third droplets in tandem catch up with the leading droplet, i.e. droplets 1 and 2 form a "pair" heading towards collision (cf. figure 6). The effective drag coefficients $C_{D,2}$ and $C_{D,3}$ are very similar, which implies that $d_{23}(t)$ stays almost constant until droplet coalescence. Ejecting the third droplet closer to the second droplet (i.e. $d_{12} = 6$ but $d_{23} = 2$) causes measurable upstream effects, as can be concluded from the solid curves in figure 7 relative to figure 6; all three droplets may coalesce if their lifetimes permit. When the second droplet is ejected closely to the leading droplet ($d_{12} = 2$) and the third droplet at $d_{23} = 6$, the last droplet becomes solitary, leaving the formation, while the first two droplets become a rapidly approaching pair (figure 8). Needless to say, systematic variations of the initial and operational conditions allows the user of the new computer simulation model to map out optimal scenarios in terms of maximum vaporization without droplet collisions.

Transient, spatially-averaged Nu values, $\overline{Nu}(t)$, for each droplet are shown in figures 9a and 9b for different Re_{d0}. Despite the relatively high initial distance ($d_{ij} = 6$), the second droplet is strongly affected by the leading droplet while the third droplet exhibits Nu values similar to the second droplet because the heat transfer mechanism is in these cases convection-dominated (cf. figures 5a–5c). Since we solve for the multiple-droplet dynamics on a droplet-by-droplet basis for each time step, the initial points $Nu_j(\tau_{G,0} \equiv 0), j = 1, 2, 3$, are suppressed and replaced with $Nu_j(0^+)$, i.e. Nu at $\tau_{G,0} = \Delta\tau_G = 10^{-5}$. Recalling that $Nu \sim \partial\theta/\partial y\,|_i$, it is transparent why the average Nu

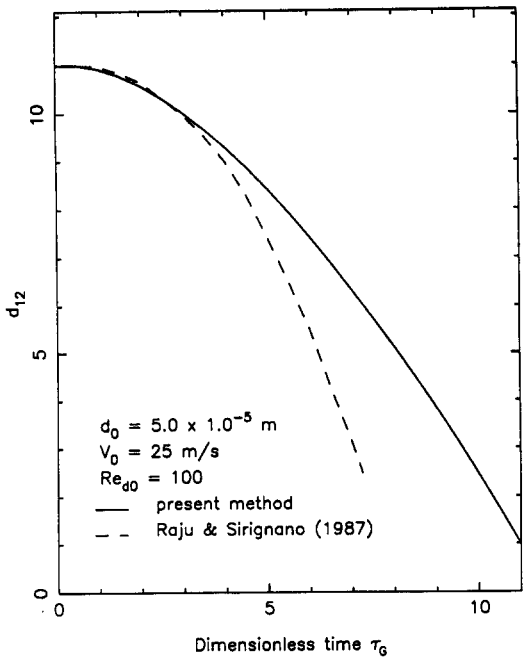

Figure 4. Comparison of droplet spacing vs time for two interacting droplets.

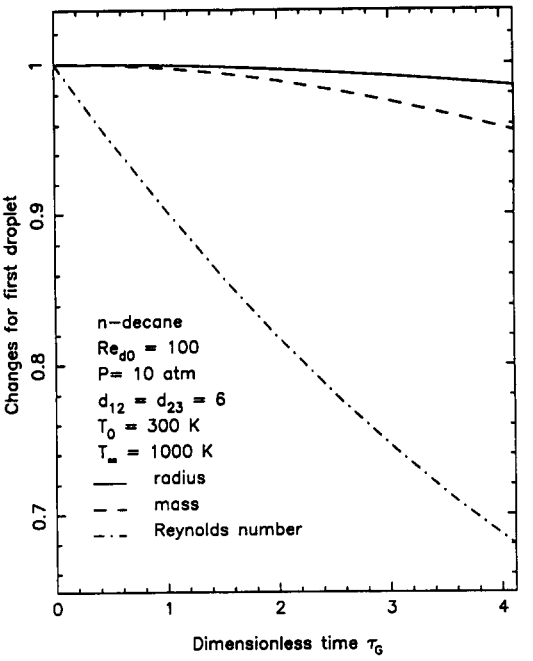

Figure 5a. Overall transient behavior of the leading droplet for three interacting droplets.

decreases with time and is higher at higher Re_d. The interfacial mass transfer or blowing velocity increases with time, generating surface temperature gradients of decreasing magnitude. With higher Re_d the thermal boundary layer becomes thinner, counteracting the gasification effect and resulting in steeper temperature gradients. Consequently, droplets vaporize faster at higher Re_d.

5. CONCLUSIONS

Accurate and efficient computer simulation of dynamically interacting droplets vaporizing on a one-dimensional trajectory is important for the basic understanding of the process dynamics and

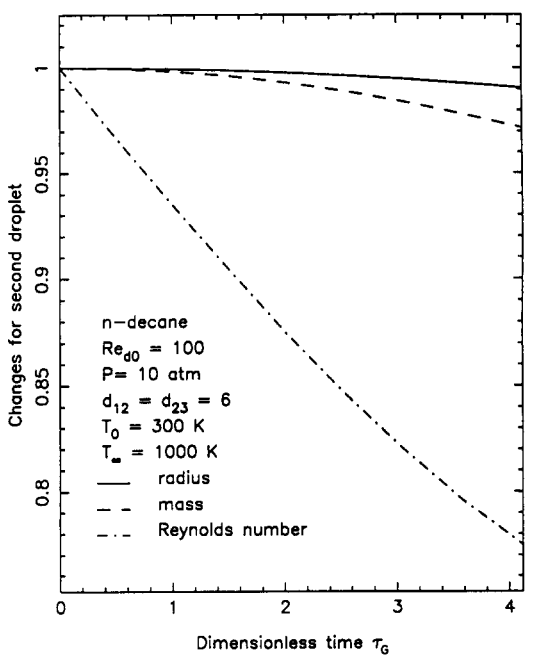

Figure 5b. Overall transient behavior of the second droplet for three interacting droplets.

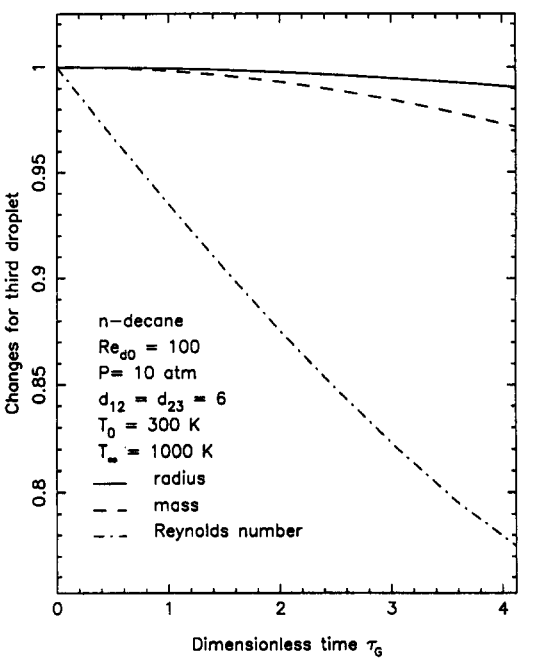

Figure 5c. Overall transient behavior of the third droplet for three interacting droplets.

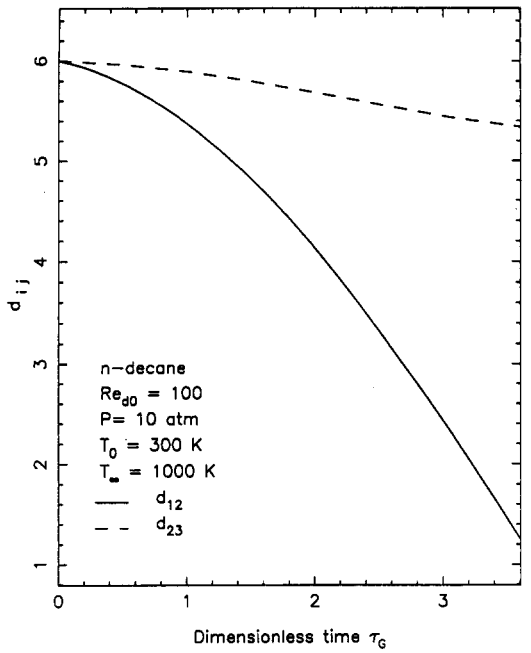

Figure 6. Droplet spacings vs time for three interacting droplets.

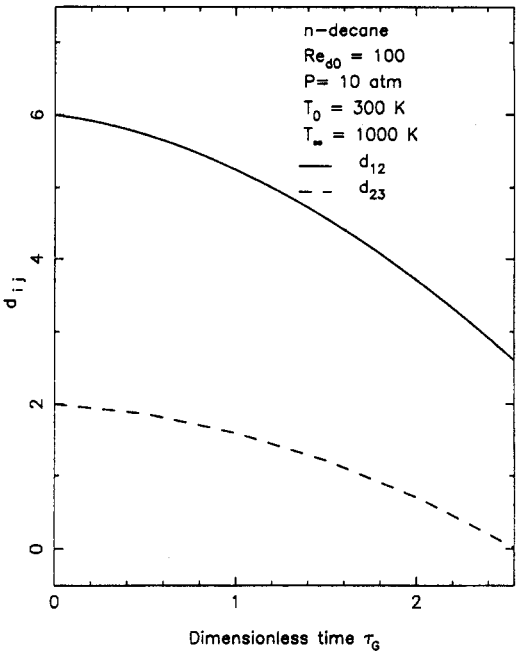

Figure 7. Droplet spacings vs time for three interacting droplets.

for improved design applications to numerous dense–dispersed flow systems. In this paper, our single vaporizing droplet analysis, using a boundary-layer type approach, is extended to study three interacting vaporizing droplets. The predictive results of the computer simulation model, previously validated with experimental data sets, compare well with an implicit finite difference solution of the full Navier–Stokes equations for laminar axisymmetric flow past two interacting vaporizing droplets.

Using input data for gasification of three *n*-decane droplets, the transient interaction effects on the individual droplet Re_d, vaporization rates or droplet shrinking, droplet distances and spatially averaged Nu values have been analyzed for different initial conditions, i.e. $Re_{d0} = 100, 200$ and

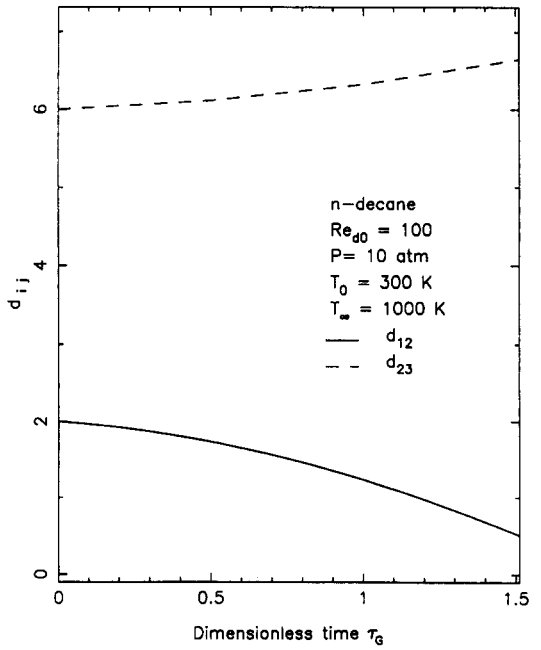

Figure 8. Droplet spacings vs time for three interacting droplets.

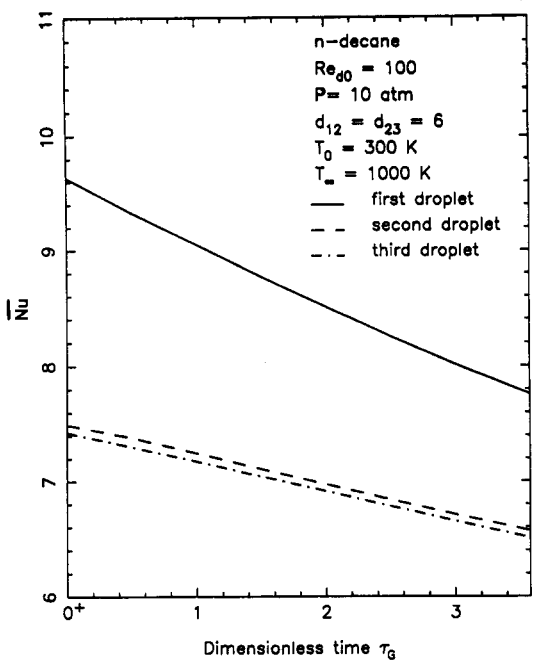

Figure 9a. Transient spatially-averaged Nu for three interacting droplets ($Re_{d0} = 100$).

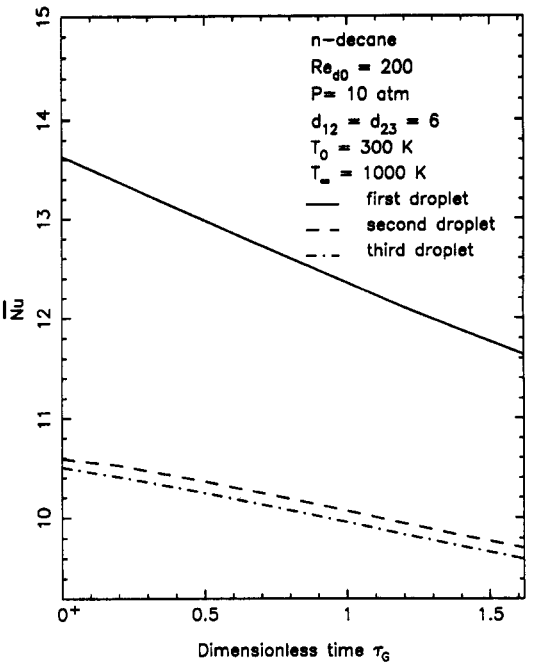

Figure 9b. Transient average Nu for three interacting droplets ($Re_{d0} = 200$).

$d_{ij,0} = 2, 4, 6$. The leading droplet always evaporates and decelerates fastest, influenced by the following droplets even when the initial distance is quite large, e.g. $d_{12} = 6$. As a result, the second droplet catches up with the first droplet rather quickly. In a multiple-droplet system, pairing is swiftly established with potential coalescence if the droplet lifetimes permit or with detachment of the third droplet which becomes solitary. The average Nu of each droplet decreases with time due to interfacial mass transfer (blowing) and increases with higher inlet Re_{d0} because of steeper interfacial temperature gradients.

The portable computer code can be used to find optimal operational conditions to achieve rapid droplet gasification without droplet collision.

Acknowledgement—This work has been supported in part by the Department of Energy, Office of Basic Energy Science; Grant No. DOE-FG05 87 ER 13728.

REFERENCES

ABRAMSON, B. & SIRIGNANO, W. A. 1988 Droplet vaporization model for spray combustion calculations. Combustion processes. Presented at the *AIAA 26th Aerospace Science Mtg*, Reno, Nev.

CLIFT, R., GRACE, J. R. & WEBER, M. E. 1978 *Bubbles, Drops and Particles*. Academic Press, New York.

DWYER, H. A. & SANDERS, B. R. 1984 Detailed computation of droplet dynamics. Presented at the *20th Int. Symp. on Combustion*, The Combustion Institute, Pittsburgh, Pa, pp. 1743–1749.

FINLAYSON, B. A. & OLSON, J. W. 1987 Heat transfer to spheres at low to intermediate Reynolds numbers. *Chem. Engng Commun.* **58**, 431–447.

KLEINSTREUER, C. & WANG, T.-Y. 1988 Heat transfer between rotating spheres and flowing power-law-fluids with suction and injection. *Int. J. Heat Fluid Flow* **9**, 328–333.

KUO, K. K. 1986 *Principles of Combustion*. Wiley-Interscience, New York.

PRAKASH, S. & KRISHAN, G. 1984 Convective droplet vaporization with transient non-convective liquid-phase heating. In *Proc. 20th Symp. on Combustion*, The Combustion Institute, Pittsburgh, Pa, pp. 1735–1742.

PRAKASH, S. & SIRIGNANO, W. A. 1980 Theory of convective droplet vaporization with unsteady heat transfer in a circulating liquid phase. *Int. J. Heat Mass Transfer* **23**, 253–268.

RAJU, M. S. & SIRIGNANO, W. A. 1987 Unsteady Navier–Stokes solution for two interacting vaporizing particles. Presented at the *AIAA 25th Aerospace Sciences Mtg*, Reno, Nev.

RAMACHANDRAN, S. & KLEINSTREUER, C. 1986 Laminar mass transfer in the wake region of closely-spaced drops. *Int. Commun. Heat Tranfer* **13,** 389–402.

RAMACHANDRAN, R. S., WANG, T. Y. & KLEINSTREUER, C. 1989a Fluid flow characteristics of three closely-spaced spheres. *AIAA Jl.* Submitted.

RAMACHANDRAN, R. S., KLEINSTREUER, C. & WANG, T. Y. 1989b Forced convection heat transfer of interacting spheres. *Numer. Heat Transfer* **A15,** 471–487.

RENKSIZBULUT, M. & HAYWOOD, R. J. 1988 Transient droplet evaporization with variable properties and internal circulation at intermediate Reynolds numbers. *Int. J. Multiphase Flow* **14,** 189–202.

ROWE, D. N. & HENWOOD, G. A. 1961 Drag forces in a hydraulic model of a fluidized bed—Part I. *Trans. Instn Chem. Engrs* **39,** 43–54.

TAL, R., LEE, D. N. & SIRIGNANO, W. A. 1984 Heat and momentum transfer around a pair of spheres in viscous flow. *Int. J. Heat Mass Transfer* **27,** 1953–1962.

THOMPSON, J. F., THAMES, F. C. & MASTIN, C. W. 1977 TOMCAT—a code for numerical generation of boundary-fitted curvilinear coordinate systems on fields containing any number of arbitrary two-dimensoinal bodies. *J. comput. Phys.* **24,** 272–302.

TSUJI, Y., MORIKAWA, Y. & TERASHIMA, K. 1982 Fluid-dynamic interaction between two spheres. *Int. J. Multiphase Flow* **8,** 71–82.

WANG, T. Y. & KLEINSTREUER, C. 1989 Laminar thermal boundary-layer flow past a vaporizing spherical droplet. *Int. J. numer. Heat Transfer*. Submitted.

WHITE, F. M. 1974 *Viscous Fluid Flow*. McGraw-Hill, New York.

ZAPRYANOV, Z. D. & TOSHEV, E. T. 1986 Hydrodynamics and heat transfer around two separated spherical particles. In *Proc. 8th Int. Conf. on Heat Transfer*, San Francisco, Calif., Vol. 5, pp. 2549–2553.